Twistronics: Manipulating the electronic properties of two-dimensional layered structures through their twist angle

Stephen Carr,[1] Daniel Massatt,[2] Shiang Fang,[1] Paul Cazeaux,[2] Mitchell Luskin,[2] and Efthimios Kaxiras[1,3]
[1]*Department of Physics, Harvard University, Cambridge, Massachusetts 02138, USA*
[2]*School of Mathematics, University of Minnesota, Minneapolis, Minnesota 55455, USA*
[3]*John A. Paulson School of Engineering and Applied Sciences, Harvard University, Cambridge, Massachusetts 02138, USA*
(Received 2 November 2016; published 17 February 2017)

The ability in experiments to control the relative twist angle between successive layers in two-dimensional (2D) materials offers an approach to manipulating their electronic properties; we refer to this approach as "twistronics." A major challenge to theory is that, for arbitrary twist angles, the resulting structure involves incommensurate (aperiodic) 2D lattices. Here, we present a general method for the calculation of the electronic density of states of aperiodic 2D layered materials, using parameter-free Hamiltonians derived from *ab initio* density-functional theory. We use graphene, a semimetal, and MoS_2, a representative of the transition-metal dichalcogenide family of 2D semiconductors, to illustrate the application of our method, which enables fast and efficient simulation of multilayered stacks in the presence of local disorder and external fields. We comment on the interesting features of their density of states as a function of twist angle and local configuration and on how these features can be experimentally observed.

DOI: 10.1103/PhysRevB.95.075420

I. INTRODUCTION

A few short years after the experimental demonstration of the existence of monolayer graphene [1], many other two-dimensional (2D) materials have been successfully fabricated [2–6]. Although single-layer 2D systems have intriguing physical properties, there has also been great interest in developing and understanding artificial heterostructures composed of multiple atomic layers weakly bonded by van der Waals forces [7]. Mechanical or chemical exfoliation and positioning of one layer on top of another allows for a relative twist between successive layers, which can destroy the alignment and thereby break the translational symmetry in the combined system [8,9]. The resulting structures may have commensurate stacking for special orientations, but more generally are incommensurate. This allows for interesting new behavior: studies of bilayer graphene have found clear twist-dependent features in both the electronic density of states and the conductivity [10,11]; at very small twist angles, a domain-wall phase appears, related to the stacking configuration [12]. Similar effects may occur in transition-metal dichalcogenide (TMDC) semiconductors, with their band gaps affected by the substrate and the relative twist-angle orientation [13]. Incommensurate structures pose a great challenge to theoretical studies since the standard description of solids with crystalline order, a periodic Bravais lattice and the associated Bloch states of electrons, is entirely absent in the combined system although each layer may still be a perfect 2D crystal.

In the effort to capture the physics of incommensurate systems, a simple approximation is to consider large supercells that can mimic the incommensurate system; in the case of first-principles calculations like density functional theory (DFT), that can afford relatively small cells, this approximation limits the physical system rather severely to special values of the twist angle [11]. This leaves important questions unaddressed: Are there distinct physical characteristics that distinguish the incommensurate from the commensurate case? Do the properties of commensurate systems approach the proper limit of the incommensurate systems as the twist angle is varied?

In the present paper we introduce a robust framework for the calculation of the properties of truly incommensurate 2D heterostructures that can address such questions for situations involving arbitrary twists between successive layers. Our method is inspired by previous mathematical works on disordered tight-binding models, which can be classified into two distinct concepts: first, an algebraic treatment of electronic transport in disordered systems [14,15] that allows for a rigorous definition of quantum-mechanical operators in a disordered material; second, the fact that local tight-binding models create exponentially localized observables, that is, they make it possible to controllably remove finite-size and edge effects from calculations [16]. We have already provided a rigorous mathematical discussion of this method [17], but here investigate its implications and results for physical systems. Our modeling is based on effective tight-binding Hamiltonians without any adjustable parameters, obtained from first-principles DFT results [18,19]. As a demonstration of the capabilities of the method, we study some prototypical systems of 2D stacked layers, including bilayer graphene, a semimetal, and bilayer MoS_2, a representative semiconductor of the TMDC family.

II. FORMALISM

We here provide a simplified discussion of the mathematical work which examines the stability and convergence of our finite-sized approach to twisted 2D material modeling [17]. The essence of our approach consists of the following ideas: A tight-binding model in d dimensions is described by localized orbitals ϕ_i in a d-dimensional lattice, $i \in \mathbb{Z}^d$, and the hopping matrix elements between them labeled t_{ij}. To describe disorder in this model, we consider the space of all possible defects and calculate physical properties for a carefully chosen subset of configurations. This is formulated by defining a configuration

space Ω with specific local configurations $\omega \in \Omega$ with a probability distribution $dP(\omega)$. Ω describes all possible environments that an atom in the infinite crystal can experience, and we simulate physical observables by sampling over this space of disordered configurations. This is in contrast to periodic approaches, which instead use the Bloch wave number, $\mathbf{k}$, as the sampling space. In incommensurate systems translational symmetry has been completely broken, and there is no Brillouin zone. Ω, referred to as the "noncommutative Brillouin zone" for this reason [14], is an alternative to this notion; neither Ω nor the Brillouin zone provide a diagonalized band structure with a finite number of eigenvalues at each point.

Viewing the interlayer interaction as a perturbative potential, the relative twist angle can be interpreted as an aperiodic disorder field applied to the single-layer system. For a fixed twist angle, the location of the orbital ϕ_i in the field created by another layer varies. This variation in location can be completely described by the offset, or shift, between the two layers' unit cells, and thus Ω can be viewed as the compact two-dimensional space of all shifts. For each shift, we construct a system of finite radius which contributes a finite-size error. The error decays exponentially with the radius, so it can be made to approach zero in a controllable fashion. Our results prove that this is a computationally feasible strategy.

In this picture, the difference between an incommensurate and commensurate twist angle becomes trivial: a commensurate angle has a finite number of possible configurations because a periodic supercell exists, while an incommensurate angle has an infinite number. If two twist angles, θ commensurate and θ' incommensurate, are extremely close then a specific shift configuration will look effectively identical between them. Therefore, the results of a single ω calculation will not vary significantly between θ and θ'; rather, it is the sampling of Ω that varies. A physical observable can show a sharp change as one varies the twist angle between commensurability and incommensurability only if it varies strongly over Ω and the commensurate twist angle does not sample Ω too finely. This distinction only holds for each layer being a perfect infinite crystal. In real materials, the difference between an incommensurate and a commensurate twist angle is less clear, as the presence of imperfections (strain, tears, ripples) may make even a commensurate system sample Ω continuously. The effect of disorder on twisted bilayer graphene's electronic properties has begun to be investigated theoretically [20,21], but we do not study it here.

Our approach can also handle other sources of disorder straightforwardly. Magnetic and electric fields can be easily introduced through a Peierls substitution or an on-site energy term, respectively. Physical defects such as vacancies, ripples, and edges are easy to implement, provided that it has been established how the hopping terms of the tight-biding Hamiltonian change in the presence of defects. This is handled by introducing extra dimensionality to Ω to represent all possible forms of disorder and applying them directly in each ω tight-binding model.

Our implementation of these ideas on a high-performance computing system is as follows.

(i) Create a heterostructure model out of layers that are disks of radius R; these disks are centered at a point with "zero shift," which is just one specific ω configuration.

(ii) Determine all relevant hopping indices H_{ij} in the sparse Hamiltonian by only looking for pairs of orbitals that are within the range of the hopping matrix elements t_{ij}.

(iii) For each desired configuration ω, displace one layer with respect to the other layer, and compute of H_{ij}^{ω} for each nonzero hopping term; from this, we then calculate the local electronic density of states (LEDoS), or any other useful physical property like the conductivity. The LEDoS is derived from the global EDoS, $g(\epsilon)$, by considering all eigenstates (indexed by s) and orbitals (indexed by x):

$$g(\epsilon) = \sum_x \frac{1}{N} \sum_{s=1}^{N} \delta(\epsilon - \epsilon_s)|\phi_s(x)|^2 = \sum_x g_x(\epsilon). \quad (1)$$

(iv) Apply the operator of interest to H_{ij}^{ω} with the kernel polynomial method (Chebyshev polynomials) [22,23]; the Chebyshev polynomials T_i form a complete basis for square integrable functions which take values in the range $[-1,1]$ and a linear combination of them can be chosen to approximate the eigenspectrum of a tight-binding Hamiltonian after a simple rescaling to ensure all eigenvalues lie in $[-1,1]$.

An additional advantage of the method is that it can be formulated into a code with excellent parallel efficiency, especially compared to DFT supercell calculations. This is a consequence of the fact that to obtain the global operator requires a large number of independent computations of the local operator in different configurations that can be run in parallel (we use MVAPICH 2.2b). Since each local operator is computed using only sparse matrix-vector operations, a second layer of parallelization can be added by using multithreaded implementations of highly optimized matrix-vector operator subroutines, which further enhances efficiency (we use Intel MKL 11.0).

III. BILAYER GRAPHENE

Twisted bilayer graphene (tBLG) provides an excellent candidate for a test of our method, since it has been well characterized by many experimental works and analytical theory [24–27]. To compute the EDoS of tBLG we used a two-band model that describes the π bonding and antibonding combinations of p_z orbitals associated with the two-atom basis of the honeycomb lattice; the tight-binding Hamiltonian is derived from first-principles calculations with the use of Wannier orbitals and involves no adjustable parameters, other than the range of hopping matrix elements [18].

The main feature of twisted bilayer graphene is the presence of van Hove singularities (VHS) above and below the Fermi energy. The origin of these VHS can be best understood by considering the low-energy band structure of tBLG as consisting of four Dirac cones at the valleys K_l and K_l', where $l = (1,2)$ labels the layers. At $\theta = 0^\circ$ twist, K_1 and K_2 are at the same point in momentum space. For $\theta > 0^\circ$, the Dirac cones move away from one another in momentum space, and a partial band-gap opening occurs where the cones now overlap. These hybridizations at the overlap of the Dirac cones produce the VHS [28], which have already been investigated by scanning tunneling microscope (STM) experiments [29–32].

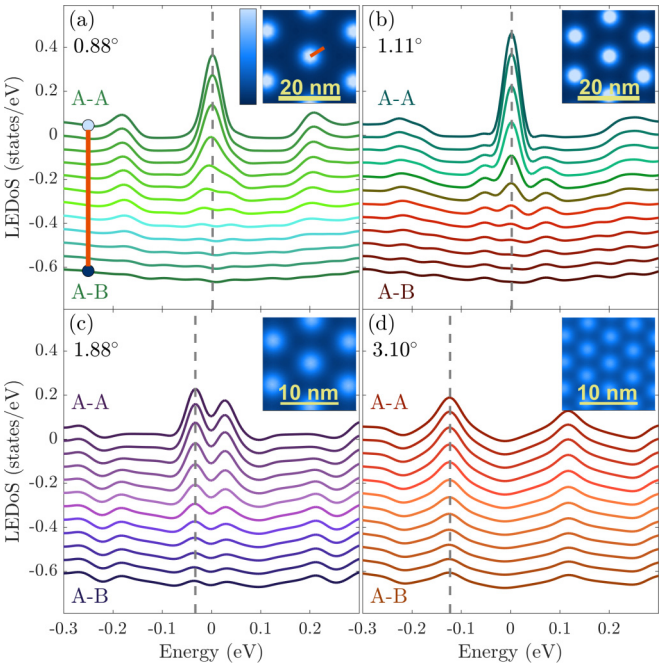

FIG. 1. Simulated local electronic density of states (LEDoS) at four different angles of twisted bilayer graphene. Each line corresponds to a different real-space configuration along the line connecting AA to AB stacking. The insets show a real-space image of the density of states in the bilayer system at the energy value identified by a dashed line. For the 0.88° angle (a) an orange line showing the AA to AB configuration path is shown in the real-space image. The figure was constructed to facilitate comparison with experiment [32], which shows excellent agreement in the positions and relative heights of the VHS. For these calculations we use a disk cutoff radius $R = 500$ Å which contains 591 344 atoms.

As a first test of the method, in Fig. 1 we compare the spatial dependence of tBLG at four twist angles to experimental results [32]. This is possible because sampling shifts over the diagonal of one layer's unit cell is the same as moving linearly from an AA to AB type stacking in the real-space moiré pattern. The simulated features of the VHS for the four selected angles are identical to those from experiment [32], but the scaling between the VHS feature and the background graphene DoS is different between theory and experiment. This can be partly explained by the fact that in STM measurements states with lower in-plane momentum $\mathbf{k}$ have shorter decay lengths [33,34]. Our method gives the DoS independent of the momentum of electronic states that contribute to it, so it is expected that the VHS will be less pronounced in experiment.

Next, we sample the configuration space Ω for a fixed twist angle of $\theta = 5.73°$ (0.1 rad) for 100 configurations along the diagonal of the unit cell (see Fig. 2). The LEDoS varies smoothly as a function of ω, with the only regions of significant configuration dependence being those near the VHS, as shown in Fig. 2(b). The AB (BA) type stacking has much lower DoS at the VHS than any other stacking configuration. Since we fit the DoS to a smooth polynomial, the divergent nature of the DoS at the VHS is only partially recovered. We can still compare the intensity of the VHS by examining its spectral weight. In Fig. 2(c) we plot the DFT ground-state energy calculations for nontwisted bilayer graphene over the same range of relative shifts. There are interesting similarities between the VHS LEDoS in (b) and the non-doped ground-state energy in (c), namely, the LEDoS at the VHS has the same dependence on relative shift as the energy. An important question is: can one controllably induce a relative twist between two graphene layers in samples of macroscopic size? We suggest that use of intercalants may facilitate this process. In particular, Li ions are known to be easily intercalated between graphene layers, with both insertion and removal being fast processes. Inspired by this observation, we have also calculated the ground-state energy as a function of relative shift for a graphene bilayer including Li-ion intercalation. In the fully lithiated structure, the relative stability of the AB and AA stacking is inverted, suggesting that Li-ion intercalation may indeed act as a way to facilitate changes in the relative twist angle even for macroscopic samples.

In Fig. 3(a) we plot the angle-dependent EDoS for tBLG. The first, second, and third VHS are visible in the low-angle regime and they move away from the Fermi level linearly with twist angle. At the VHS, we find that the real-space local DoS is highly localized at the AA stacking sites as in Fig. 1, in agreement with experimental STM results [31,35]. It is easy to identify in Fig. 3(a) the first and second "magic angles" of tBLG (near 1.1 and 0.5°, respectively), explained by band flattening near the Fermi level [24,26]. In Fig. 3(b) we plot the calculated EDoS of monolayer graphene in the presence of out-of-plane magnetic field. The Landau levels (LL's) in the monolayer and the VHS in the twisted bilayer both represent tunable, localized electronic states. This similarity may support the interpretation of the twisted interlayer interaction as a non-Abelian gauge field, the exact nature of which is still being investigated [26,32,36,37]. These calculations allow a very robust determination of the monolayer's Fermi velocity without a band-structure calculation, using the low-energy model for the LL's [28]:

$$E(n) = \pm v_F \sqrt{2eBN} \tag{2}$$

with the result for the Fermi velocity $v_F = 1.2 \times 10^6$ m/s. Finally, we test the interaction between twist and magnetic field in Fig. 3(c): at the AA stacking with a 3.1° twist there are many clear LL's and at a field of 5 T the peak of the VHS is significantly altered relative to its zero-field shape. At a twist of 1.1°, the magnetic field dependence of the peak is not visible. These results are in good agreement with experimental STM measurements [30,32].

The Streda formula [38] relates the fluctuations in the integrated electronic density n under small changes in the magnetic field strength B to the Hall conductance σ_{xy}, while the Fermi energy E of the system lies in a gapped region, $E \in E_g$:

$$\sigma_{xy} = e \frac{\partial n(E)}{\partial B}\bigg|_{E \in E_g}. \tag{3}$$

Averaging over 100 configurations of the LEDoS on both layers gives values for σ_{xy} that jump from -2 to $+2$ in units of e^2/h across the central LL in the 3.1° simulation. This change of $+4e^2/h$, before taking into account spin, corresponds to the fourfold degeneracy for the $N = 0$ LL of bilayer graphene,

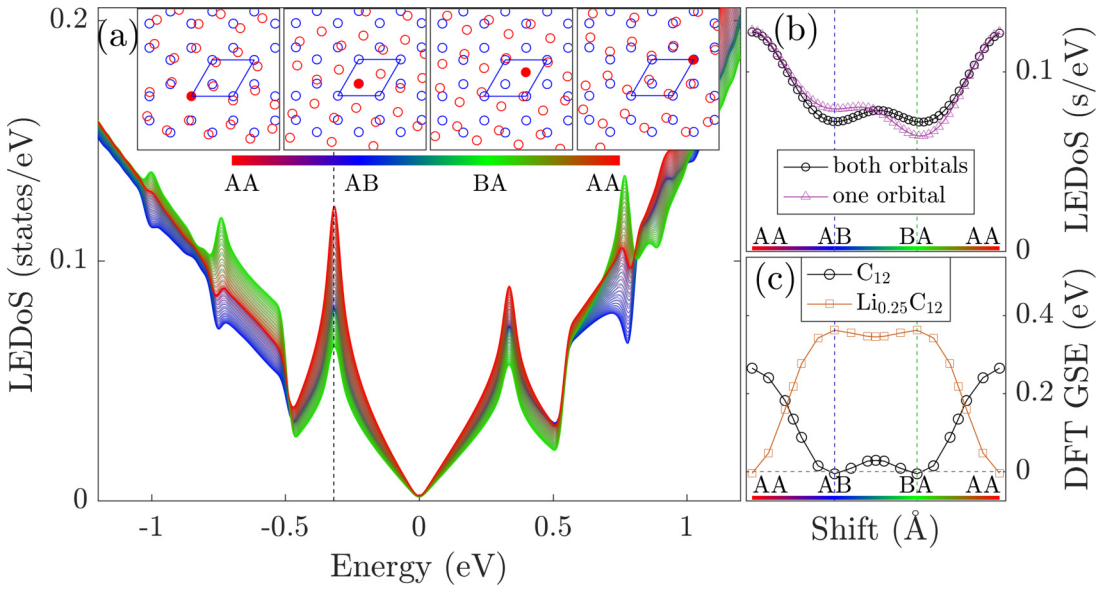

FIG. 2. Local electronic density of states as a function of shift distance across the unit-cell diagonal. (a) Scan of a single orbital's LEDoS with the coloring corresponding to distance across the diagonal. The insets show the real-space configurations ω for three types of stacking with the atoms in each layer represented by different color circles (red and blue for top and bottom). The unit cell of the bottom layer is outlined in blue and the shifted orbital is highlighted as a filled red dot. (b) LEDoS at the selected VHS peak as a function of shift for one orbital (triangles) and for the average of both orbitals (circles), which is properly symmetric. The peak varies smoothly with shift and has critical points at the three special stacking configurations. For the calculations in (a,b) we use a disk cutoff radius $R = 500$ Å which contains 591 344 atoms. (c) Ground-state energy (GSE) of $\theta = 0^\circ$ twist angle with and without Li-ion doping (see text for details).

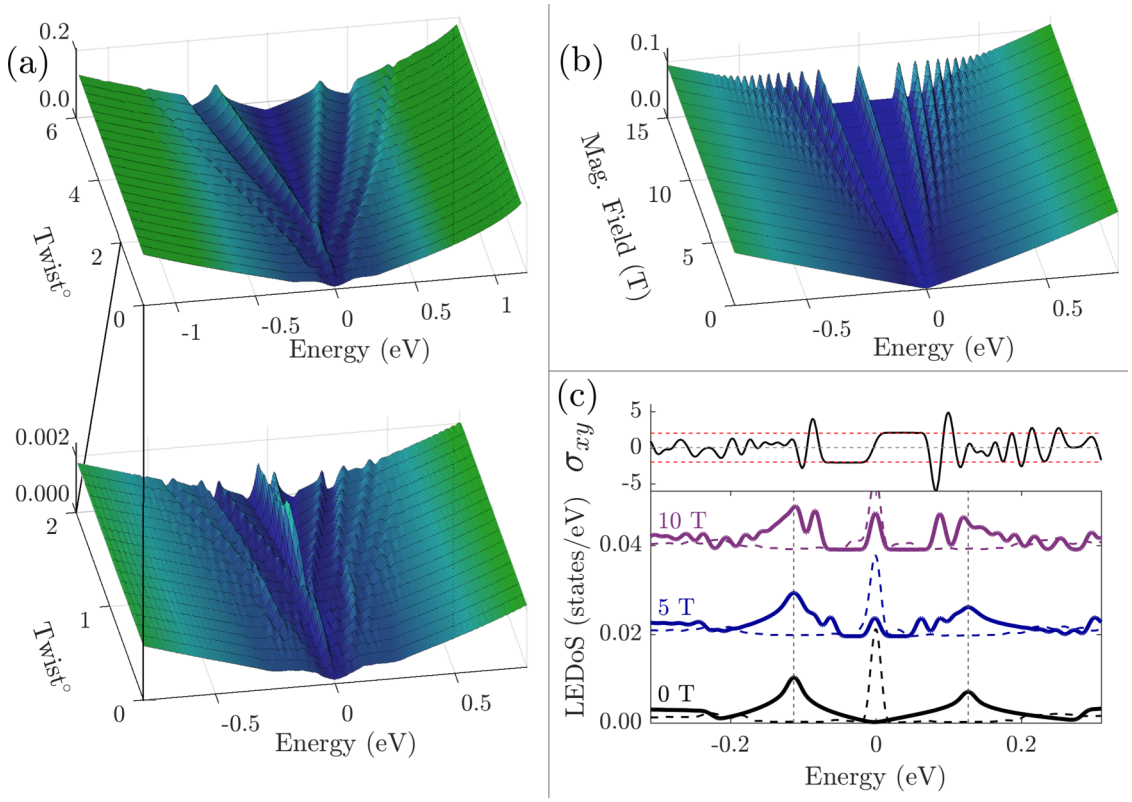

FIG. 3. (a) Average EDoS as a function of twist angle for tBLG. (b) Average EDoS for monolayer graphene in the presence of varying magnetic field. (c) LEDoS for AA stacked tBLG with 3.1° (solid line) and 1.1° (dashed line) twist angle at different values of the magnetic field and Hall conductivity σ_{xy} in units of e^2/h, with the horizontal red dashed lines at $\pm 2e^2/h$. For these calculations we use a disk cutoff radius $R = 750$ Å (1 330 550 atoms) and averages are over 100 configurations across the unit cell (10 × 10 grid).

with the four states originating from the monolayer's K, K' valley degeneracy (factor of 2) and the two sheets (another factor of 2). A change of $+8e^2/h$ is observed in experiment for tBLG, which is in agreement with our results when we take into account spin degeneracy [8]. If only the AA configuration is used in the calculation we do not obtain good quantization of σ_{xy}. Just like integrating over the entire Brillouin zone when computing in momentum space, integrating over the entire configuration space Ω is required in the case of tBLG. This allows us to compute the Chern number for the wave functions in the gapped region by taking the difference in σ_{xy} in units of the conductance quanta ($+4e^2/h$), which indicates that our method can capture accurately certain topological properties of the electronic band structure.

IV. BILAYER TMDC

Unlike bilayer graphene, transition-metal dichalcogenides will not be well described by low-energy theory due to their large band gaps (about 2 eV). For bilayers of TMDCs we use an 11 band model, consisting of five d orbitals on the transition-metal atom and three p orbitals on each of the two chalcogen atoms [19]. The interlayer interaction is modeled only between the chalcogen atoms closest to the bilayer interface. Here we present results for MoS_2, the model Hamiltonian of which includes the GW approximation for more accurate representation of the electronic structure. Since we are mainly interested in studying twist-angle dependent effects, we will neglect spin polarization, but an *ab initio* model with spin-orbit coupling can be easily substituted if such effects are important.

Some twist-angle dependent features were seen in the LEDoS for both WSe_2 and MoS_2, but most were not near the conduction- or valence-band edges. The twist-angle dependence of the density of states for bilayer MoS_2 is shown in Fig. 4(a). There are significant changes in the EDoS deep into the valence band (more than 2 eV below the maximum), but it is difficult to probe this region experimentally. They could be observed as interesting properties for high-frequency conductivity or optical activity.

Instead, we focus on the valence- and conduction-band edges. The band gap is a twist-angle dependent feature: it increases by 76 meV (a ~4% change) going from 0 to 28.6° twist angle. The regions near the valence- and conduction-band extrema are shown in great detail in Figs. 4(b) and 4(c), with the logarithmic scale showing the changes more clearly. These plots also show the good numerical convergence of the EDoS in our model, with noticeable numeric error only occurring when the EDoS is smaller than 10^{-5} states per eV. This error, reminiscent of Gibbs oscillations [22], is likely an artifact of the kernel polynomial method (KPM) attempting to fit a smooth function to a band edge in the eigenvalue spectrum. We thus take a region about 10^{-4} states per eV to compare changes in the band gap (plotted in orange). Our model does not take into account changes in the distance between the two layers as a function of twist angle, which could give additional dependence of the band gap and can be incorporated as a dependence of the tight-binding hopping matrix elements on twist angle and distance.

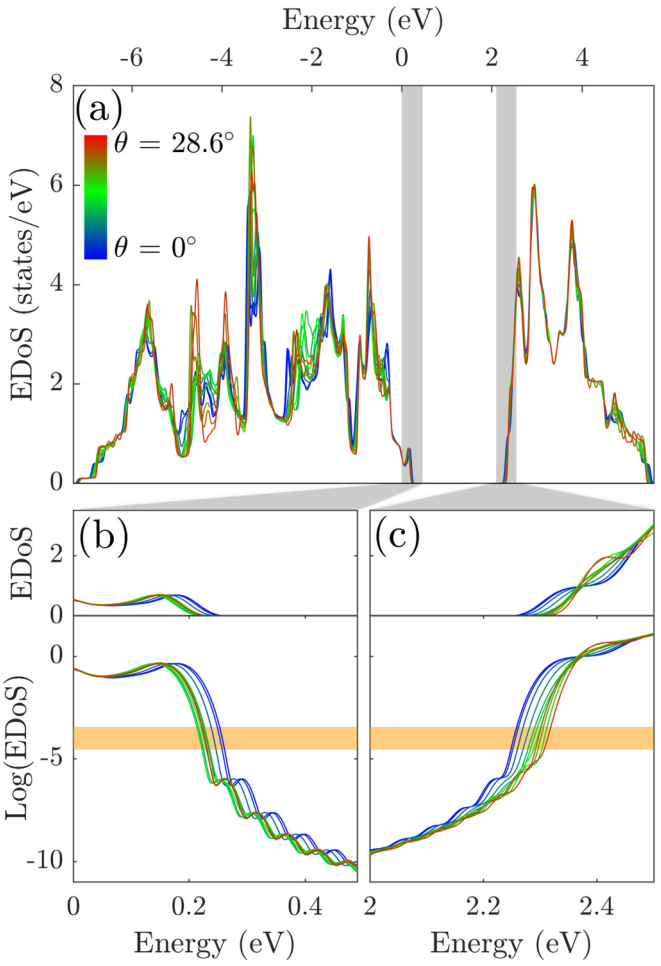

FIG. 4. (a) EDoS for twisted bilayer MoS_2 from 0° (blue) to 28.65° (red) twist angle. (b) and (c) EDoS near the valence- and conduction-band extrema, with the logarithmic scales showing the changes in greater detail. These calculations use a disk cutoff radius $R = 300$ Å (193 700 atoms) and are averaged over 100 configurations across the unit cell (10×10 grid).

V. CONCLUSION

We have introduced a method for parameter-free computation of electronic properties in incommensurate layered 2D materials with controllable errors. Although here we have only studied bilayer materials, the method is general and extends to any number of layers and of arbitrary heterostructure composition. Viewing the problem on the space of configurations, Ω, allows us to fully characterize the properties of incommensurate (aperiodic) systems. The method allows for the inclusion of external fields and other sources of disorder, such as strain or defects. We present results of applying the method to twisted bilayer graphene and a representative of the TMDC family of semiconductors. The method is accurate enough to correctly calculate quantization of Hall conductivity in tBLG in the presence of magnetic fields, and reproduces the correct Chern number for the $N = 0$ Landau level. It also predicts that bilayer TMDC's have a twist-dependent band gap. The method is a promising candidate for the targeted design of electronic properties in layered heterostructures.

ACKNOWLEDGMENTS

We acknowledge S. Shirodkar for providing the Li-ion itercalated graphene calculations shown in Fig. 2(c) and B.I. Halperin and D. Huang for helpful discussions. The computations in this paper were run on the Odyssey cluster supported by the Faculty of Arts & Sciences Division of Science, Research Computing Group at Harvard University. This work was supported by the ARO MURI Award No. W911NF-14-0247. S. Fang is supported by the Science and Technology Center for Integrated Quantum Materials, NSF Grant No. DMR-1231319.

[1] K. S. Novoselov, A. K. Geim, S. V. Morozov, D. Jiang, Y. Zhang, S. V. Dubonos, I. V. Grigorieva, and A. A. Firsov, Science **306**, 666 (2004).

[2] A. Ayari, E. Cobas, O. Ogundadegbe, and M. S. Fuhrer, J. Appl. Phys. **101**, 014507 (2007).

[3] C. R. Dean, A. F. Young, I. Meric, C. Lee, L. Wang, S. Sorgenfrei, K. Watanabe, T. Taniguchi, P. Kim, K. L. Shepard, and J. Hone, Nat. Nanotechnol. **5**, 722 (2010).

[4] K. F. Mak, C. Lee, J. Hone, J. Shan, and T. F. Heinz, Phys. Rev. Lett. **105**, 136805 (2010).

[5] B. Radisavljevic, A. Radenovic, J. Brivio, V. Giacometti, and A. Kis, Nat. Nanotechnol. **6**, 147 (2011).

[6] D. De, J. Manongdo, S. See, V. Zhang, A. Guloy, and H. Peng, Nanotechnology **24**, 025202 (2013).

[7] A. K. Geim and I. V. Grigorieva, Nature (London) **499**, 419 (2013).

[8] Y. Cao, J. Y. Luo, V. Fatemi, S. Fang, J. D. Sanchez-Yamagishi, K. Watanabe, T. Taniguchi, E. Kaxiras, and P. Jarillo-Herrero, Phys. Rev. Lett. **117**, 116804 (2016).

[9] E. Koren, I. Leven, E. Lörtscher, A. Knoll, O. Hod, and U. Duerig, Nat. Nanotechnol. **11**, 752 (2016).

[10] A. Rozhkov, A. Sboychakov, A. Rakhmanov, and F. Nori, Phys. Rep. **648**, 1 (2016).

[11] K. Uchida, S. Furuya, J.-I. Iwata, and A. Oshiyama, Phys. Rev. B **90**, 155451 (2014).

[12] C. R. Woods, L. Britnell, A. Eckmann, R. S. Ma, J. C. Lu, H. M. Guo, X. Lin, G. L. Yu, Y. Cao, R. V. Gorbachev, A. V. Kretinin, J. Park, L. A. Ponomarenko, M. I. Katsnelson, Y. N. Gornostyrev, K. Watanabe, T. Taniguchi, C. Casiraghi, H.-J. Gao, A. K. Geim, and K. S. Novoselov, Nat. Phys. **10**, 451 (2014).

[13] A. Ebnonnasir, B. Narayanan, S. Kodambaka, and C. V. Ciobanu, Appl. Phys. Lett. **105**, 031603 (2014).

[14] J. Bellissard, A. van Elst, and H. Schulz-Baldes, J. Math. Phys. **35**, 5373 (1994).

[15] E. Prodan, Appl. Math. Res. Express **2013**, 176 (2012).

[16] H. Chen and C. Ortner, SIAM Multiscale Model. Simul. **14**, 232 (2016).

[17] D. Massatt, M. Luskin, and C. Ortner, arXiv:1608.01968.

[18] S. Fang and E. Kaxiras, Phys. Rev. B **93**, 235153 (2016).

[19] S. Fang, R. Kuate Defo, S. N. Shirodkar, S. Lieu, G. A. Tritsaris, and E. Kaxiras, Phys. Rev. B **92**, 205108 (2015).

[20] A. O. Sboychakov, A. L. Rakhmanov, A. V. Rozhkov, and F. Nori, Phys. Rev. B **92**, 075402 (2015).

[21] A. V. Rozhkov, A. O. Sboychakov, A. L. Rakhmanov, and F. Nori, Phys. Rev. B **95**, 045119 (2017).

[22] A. Weiße, G. Wellein, A. Alvermann, and H. Fehske, Rev. Mod. Phys. **78**, 275 (2006).

[23] E. Di Napoli, E. Polizzi, and Y. Saad, Numerical Linear Algebra with Applications **23**, 674 (2016).

[24] R. Bistritzer and A. H. MacDonald, Proc. Natl. Acad. Sci. USA **108**, 12233 (2011).

[25] E. J. Mele, Phys. Rev. B **84**, 235439 (2011).

[26] P. San-Jose, J. González, and F. Guinea, Phys. Rev. Lett. **108**, 216802 (2012).

[27] J. M. B. Lopes dos Santos, N. M. R. Peres, and A. H. Castro Neto, Phys. Rev. B **86**, 155449 (2012).

[28] A. H. Castro Neto, F. Guinea, N. M. R. Peres, K. S. Novoselov, and A. K. Geim, Rev. Mod. Phys. **81**, 109 (2009).

[29] G. Li, A. Luican, J. M. B. Lopes dos Santos, A. H. Castro Neto, A. Reina, J. Kong, and E. Y. Andrei, Nat. Phys. **6**, 109 (2009).

[30] A. Luican, G. Li, A. Reina, J. Kong, R. R. Nair, K. S. Novoselov, A. K. Geim, and E. Y. Andrei, Phys. Rev. Lett. **106**, 126802 (2011).

[31] D. Wong, Y. Wang, J. Jung, S. Pezzini, A. M. DaSilva, H.-Z. Tsai, H. S. Jung, R. Khajeh, Y. Kim, J. Lee, S. Kahn, S. Tollabimazraehno, H. Rasool, K. Watanabe, T. Taniguchi, A. Zettl, S. Adam, A. H. MacDonald, and M. F. Crommie, Phys. Rev. B **92**, 155409 (2015).

[32] L.-J. Yin, J.-B. Qiao, W.-J. Zuo, W.-T. Li, and L. He, Phys. Rev. B **92**, 081406 (2015).

[33] J. A. Stroscio, R. M. Feenstra, and A. P. Fein, Phys. Rev. Lett. **57**, 2579 (1986).

[34] D. Huang, C.-L. Song, T. A. Webb, S. Fang, C.-Z. Chang, J. S. Moodera, E. Kaxiras, and J. E. Hoffman, Phys. Rev. Lett. **115**, 017002 (2015).

[35] I. Brihuega, P. Mallet, H. González-Herrero, G. Trambly de Laissardière, M. M. Ugeda, L. Magaud, J. M. Gómez-Rodríguez, F. Ynduráin, and J.-Y. Veuillen, Phys. Rev. Lett. **109**, 196802 (2012).

[36] W.-Y. He, Y. Su, M. Yang, and L. He, Phys. Rev. B **89**, 125418 (2014).

[37] M. Van der Donck, F. M. Peeters, and B. Van Duppen, Phys. Rev. B **93**, 247401 (2016).

[38] P. Streda, J. Phys. C **15**, 1299 (1982).